Vortex dynamics in triangular-shaped confining potentials

Andreas Vogel,[1,a)] Anna Corinna Niemann,[1] Charlotte Stenner,[1] André Drews,[1,2] Mi-Young Im,[3] Peter Fischer,[3] and Guido Meier[1]
[1]*Institut für Angewandte Physik und Zentrum für Mikrostrukturforschung, Universität Hamburg, 20355 Hamburg, Germany*
[2]*Arbeitsbereich Technische Informatik Systeme, Universität Hamburg, 22527 Hamburg, Germany*
[3]*Center for X-Ray Optics, Lawrence Berkeley National Laboratory, Berkeley, California 94720, USA*

Triangular-shaped permalloy microstructures in the vortex magnetization state are studied via transmission soft x-ray microscopy, broadband-ferromagnetic resonance measurements, and micromagnetic simulations. The vortex chirality can be controlled via the direction of a saturating in-plane magnetic field applied before nucleation of the vortex state. The resonance frequencies of vortex gyration are probed for different equilibrium positions within the magnetic structure to determine the shape of the asymmetric confining potential. The experimental results are shown to coincide with micromagnetic simulations.

Collective spin excitations on the subnanosecond timescale and a variety of potential technological applications give rise to a broad scientific interest in the dynamic properties of ferromagnetic microstructures with vortex magnetization configuration.[1–5] The vortex state is characterized via the core polarization ($p = \pm 1$) indicating the magnetization orientation of the core and the chirality ($C = \pm 1$) describing the direction of the in-plane curling magnetization around the core. An additional perpendicular magnetic field during nucleation,[6] pulsed magnetic fields[7] or spin-polarized currents,[8] and spin waves[9] can be used to manipulate the core polarization. Regular polygonal structures with an odd number of edges also allow to control the chirality via an in-plane magnetic field.[10–12] Once deflected and released, vortices exhibit a spiral motion around their equilibrium position, where the polarization determines the intrinsic sense of gyration. This low frequency mode of gyration can be resonantly excited by alternating magnetic fields[13] or spin-polarized currents.[14] An excitation can be transferred via dipolar interaction between neighboring ferromagnetic elements with the transfer efficiency strongly depending on their separation and the relative configurations of the vortex states.[15–17] In this context, potential applications in information-signal processing devices or magnonic crystals have been discussed.[18–20] Due to their geometry, triangular structures allow a very small distance between the neighboring structures and the design of a variety of complex systems from chains[21] to deterministic fractals[22] each with a unique dynamic behavior. For further development, it is crucial to investigate the dynamic properties of the magnetic vortex in a triangle under the influence of various internal and external parameters. As a first step, Miyata *et al.*[23] detected the resonance frequency of spin-torque driven vortex core gyration in a triangular structure at zero field using a homodyne detection technique.

Here, we show that the chirality in micron-sized permalloy triangles can be controlled via an external magnetic field. Non-invasive transmission soft x-ray microscopy is used to determine the in-plane magnetization configuration depending on a magnetic field applied in the plane of the sample surface. The asymmetric magnetic confining potential is investigated using micromagnetic simulations of the free vortex relaxation and resonant excitation of vortex-core gyration in broadband-ferromagnetic resonance (FMR) measurements for different equilibrium positions within the magnetic structure. It is shown that the shape of the triangle is reflected in the shape of the confining potential.

For x-ray microscopy, equilateral triangles with an edge length of 2 μm are prepared by electron-beam lithography and lift-off processing. Polycrystalline permalloy ($Ni_{80}Fe_{20}$) with a thickness of 50 nm is thermally evaporated onto 150 nm thin silicon-nitride membranes. The measurements are performed at beamline 6.1.2 of the Advanced Light Source in Berkeley, CA, USA.[24] Magnetic contrast is provided via the magnetic circular dichroism effect at the Ni L_3-absorption edge.[25] The sample is illuminated with circularly polarized x-rays having an incident energy of 852.7 eV. The sample surface is mounted at an angle of 60° relative to the beam direction to be sensitive to the in-plane magnetization direction along the x axis. Figure 1 shows exemplary differential x-ray images of single triangles at different magnetic bias fields. In Fig. 1(a), the triangle has been saturated along the x axis in an external field of $\mu_0 H_{sat} = -120$ mT that is subsequently reversed in steps of 6 mT. The vortex core in the triangle with a clockwise curling magnetization ($C = -1$) is displaced in positive y direction towards the top of the structure under the application of a field in positive x direction. The core is annihilated at a field of 36 mT. Due to asymmetric nucleation energies for the clockwise and counterclockwise chiralities, the chirality can be controlled via the initial magnetization direction of the uniformly magnetized state. Figures 1(b)–1(d) show the vortex magnetization configurations achieved after saturation

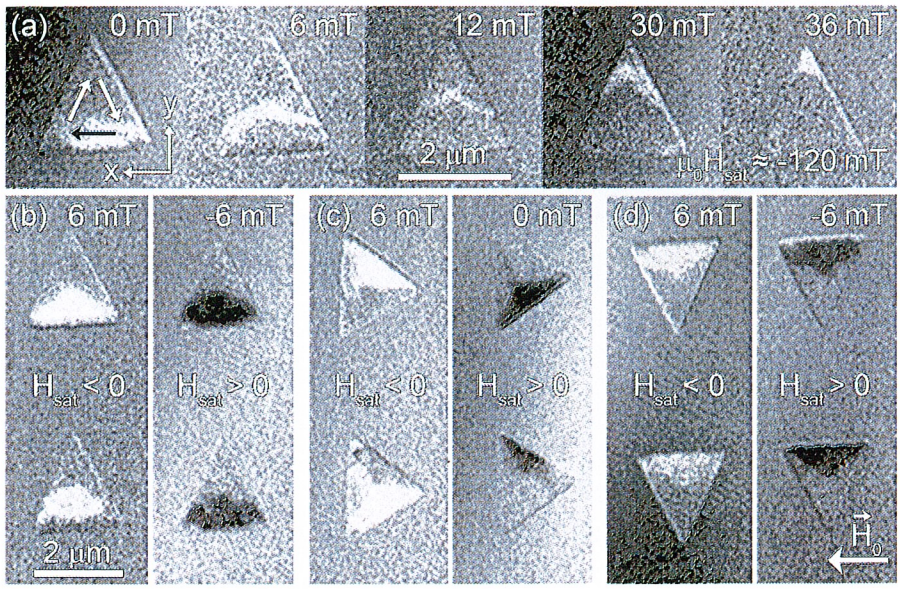

FIG. 1. Differential magnetic transmission x-ray micrographs with respect to the preceding field step. Positive field values correspond to a magnetic field $\vec{H}_0$ applied in positive x direction. White (black) contrast corresponds to the magnetization pointing in positive (negative) x direction. Arrows inside the first triangle in (a) illustrate the magnetization directions of the three magnetic domains. In (b)-(d), the sample has been primarily saturated in the indicated field direction parallel to the x axis.

for different tilting angles between the base of the triangle and the magnetic field axis. Overall, 101 triangles with tilting angles between 0° and 60° in steps of 5° have been measured several times each. Note that the vortex state typically nucleates at small opposing fields. However, also nucleation at zero field occurs, see Figs. 1(a) and 1(c). In accordance with the magnetic-force microscopy images by Yakata *et al.*[10] and Jaafar *et al.*,[12] the magnetization direction of the domain at the base opposes the direction of the magnetic field used to saturate the sample when one edge of the triangle is almost parallel to the field axis. The same ground state is reproducibly obtained, compare Figs. 1(b) and 1(d). Inverting the saturating field yields the opposite chirality. Both chiralities are possible when an edge of the equilateral triangle is oriented perpendicular to the field axis, see Fig. 1(c). The same results have been obtained for triangles with an edge length of 1 μm (not shown).

To investigate the vortex dynamics, arrays of 4×100 (=400) equilateral triangles with an edge length of 1.5 μm and a thickness of 50 nm are prepared on a silicon substrate with a 300 nm silicon-oxide coating. The spacing between neighboring structures is 3 μm to prevent coupling via the in-plane stray fields.[6] A coplanar waveguide is deposited on top of the triangles by dc magnetron sputtering of 120 nm gold. The signal line splits into four 1.5 μm wide lines each aligned with the centers of the triangles, see Fig. 2(a). Transmission spectra are measured at room temperature by means of a broadband FMR setup using a vector-network analyzer.[26] A sinusoidal signal is driven through the signal line leading to an alternating magnetic field of about 0.4 mT which acts parallel to the y axis. Figure 2(b) shows FMR transmission spectra taken at static bias fields from $\mu_0 H_0 = -30$ mT to 30 mT parallel to the waveguide. Prior to each field step, the vortex magnetization configuration in each triangle is reset to $C = -1$ via saturation of the sample along the x axis with $\mu_0 H = -90$ mT and subsequent application of a field of 7 mT pointing in the opposite direction. Energy absorption due to resonant excitation of the vortex-core gyration by the alternating magnetic field is observed as a reduction of transmission in the FMR spectra, as shown in Fig. 2(c). For small deflections from the equilibrium position at zero field, the vortex core can be treated as a quasiparticle in a two-dimensional harmonic potential.[27,28] An in-plane bias field leads to a translation of the equilibrium position of

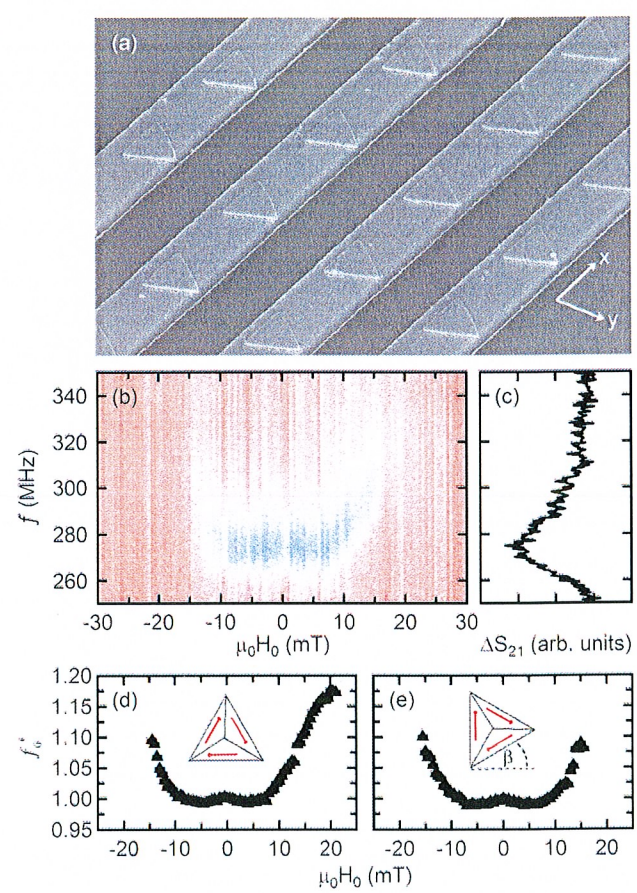

FIG. 2. (a) Scanning-electron micrograph of an ensemble of triangular structures covered by the signal line of a coplanar waveguide splitted into four separated lines. (b) Broadband-ferromagnetic resonance transmission spectra of the ensemble shown in (a). An external bias field along the x axis is successively increased from $\mu_0 H_0 = -30$ mT to 30 mT. The dark (blue) color corresponds to reduced transmission. (c) Spectrum at zero bias field. The normalized resonance frequencies versus bias field is shown for triangles (d) aligned with the x axis and (e) tilted by $\beta = 30°$ with respect to the x axis.

the core within the triangle. Figure 2(d) shows the resonance frequency of vortex gyration as a function of the bias field normalized with the resonance frequency at zero field. The measurements reveal an asymmetry around zero field. At negative bias fields, the resonant vortex excitation can be detected down to -14 mT where the resonance frequency is increased by 10%. At positive bias fields, the signal can be clearly observed up to 20 mT where the resonance frequency is increased by 17%. The change in the resonance frequency indicates deviations from the parabolic potential where a higher frequency corresponds to a steeper potential.[29–32] Since the studied triangles have a clockwise curling magnetization ($C = -1$), at positive bias fields along the x axis the vortex core is pushed towards the upper corner of the triangle, compare Fig. 1(a). At negative bias fields, the vortex is displaced into the direction of the triangle's base. Tilting the triangles by $\beta = 30°$ with respect to the x axis leads to a different field dependence of the resonance frequency, see Fig. 2(e). Note that the bias field is still applied parallel to the waveguide that is aligned with the x axis. In this case, a symmetric shift in the resonance frequency around zero field can be observed which is expected from symmetry considerations. According to the x-ray measurements, the ensemble of the tilted triangles consists of triangles with both chiralities. The inset in Fig. 2(e) only exemplarily shows one of the two possible configurations.

To get a better understanding of the potential landscape, bias fields between 9 mT and 15 mT are applied under different angles θ between 0° and 180° with respect to the x axis, illustrated in the row above Fig. 3(a). Figure 3(a) shows the corresponding resonance frequencies determined from FMR measurements on an ensemble of triangles with $\beta = 0°$, compare Figs. 2(d) and 2(e). The magnetic confining potential reflects the shape of the triangular structure. For the same absolute value of the bias field, the potential at the corners of the triangle is steeper than the potential at the edges of the triangle. Increasing the strength of the bias field leads to an even more pronounced difference in the potentials at an equilibrium position shifted towards the corner or towards the edge of the structure. For a bias field of 15 mT, the vortex is already annihilated close to the edge, compare Fig. 2(b), and thus no resonant vortex excitation can be observed. In a recent publication by Langner *et al.*,[31] strongly elongated vortex-core trajectories at resonance have been reported for an equilibrium position close to the edge of a ferromagnetic square. The long semiaxis of the trajectory has been observed to lie almost parallel to the edge. Considering such a shape of the trajectory allows to give a reasonable explanation for the difference in the resonance frequencies, e.g., between a field angle of 60° and 180° at a bias field of 12 mT which is not expected from symmetry considerations. One has to keep in mind that the exciting linearly polarized rf field always points parallel to the y axis. Thus, it acts along the short semiaxis of the trajectory at a field angle of 180° and at an angle of 30° with respect to the long semiaxis at a field angle of 60°. Figure 3(b) reveals that tilting of the triangles by small angles β leads to a shift of the resonance frequency at a bias field around 12 mT as a function of the field angle θ. As a guide to the eye, dashed lines indicate the position of the minima which is shifted consistently with

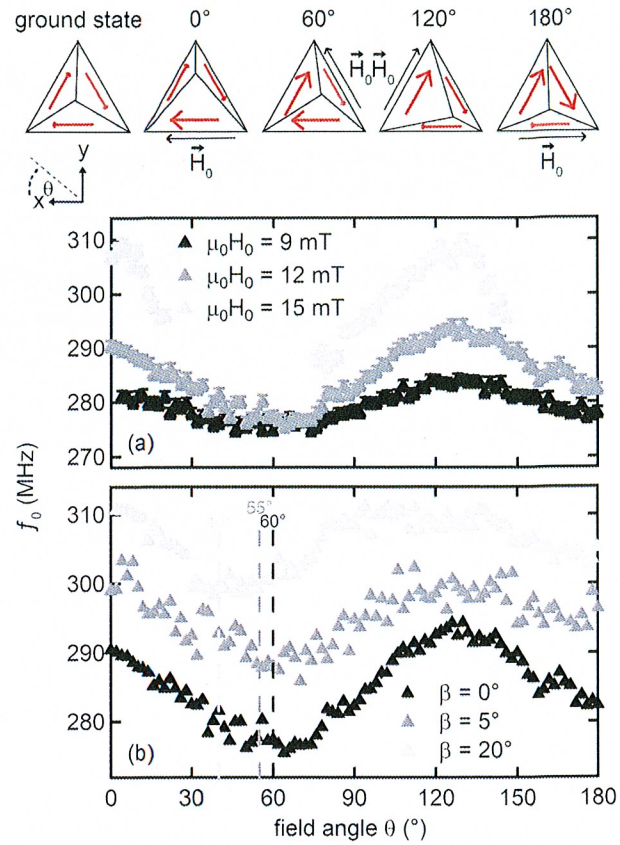

FIG. 3. (a) Resonance frequency f_0 of vortex gyration as a function of the strength of the external bias field $\vec{H}_0$ and its angle θ with respect to the x axis determined from broadband FMR measurements. The position of the vortex core in a triangle with $C = -1$ for characteristic field angles is illustrated on top of (a). (b) Dependence of the resonance frequency on the field angle at a bias field of about 12 mT for ensembles of triangles tilted by different angles β. For clarity, the curves in (b) are successively offset.

the tilting angle β. It should be noted that x-ray measurements have clearly shown a preferred chirality of $C = -1$ after saturation in negative x direction for triangles tilted by $\beta = 5°$ and $\beta = 20°$ (not shown).

In addition, micromagnetic simulations of the free relaxation after initial deflection of the vortex core in a single equilateral triangle with an edge length of 1.5 μm and a thickness of 50 nm are performed using the Micromagnum code[29,33] with a cell size of $4 \times 4 \times 50\,\text{nm}^3$. Typical parameters for permalloy, e.g., a saturation magnetization $M_S = 8 \times 10^5\,\text{Am}^{-1}$, an exchange constant $A = 13 \times 10^{-12}\,\text{Jm}^{-1}$, and a Gilbert damping parameter $\alpha = 0.01$ are taken. The eigenfrequencies as a function of the strength of the external bias field and the field angle θ shown in Fig. 4(a) are determined via fitting of the vortex trajectories. In the case of low damping, the deviation between the eigenfrequency and the frequency of resonant excitation is sufficiently small to allow direct comparison to the experiments. The simulation results reproduce the experimental results for the corresponding field values and field angles with a quantitative deviation of at most 10%, compare Figs. 3(a) and 4(a). In contrast to the experiments, vortex gyration can be still observed for all field angles at a bias field of 15 mT. The difference in the frequencies, e.g., for field angles of 60° and 180° attributed to the linearly polarized excitation in the FMR measurements is consequently not observed in the

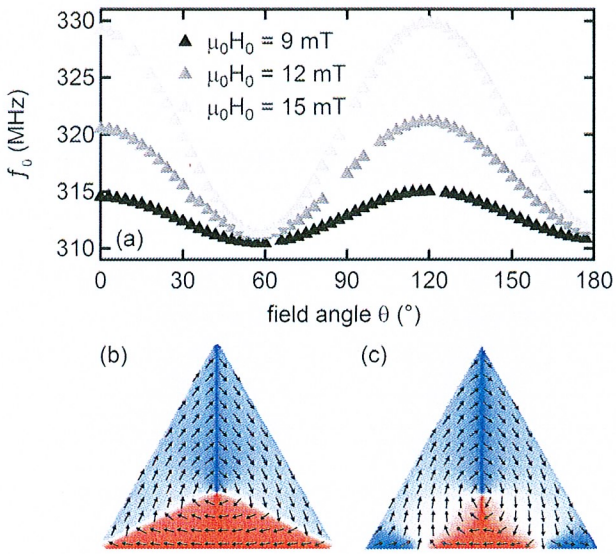

FIG. 4. (a) Eigenfrequency f_0 of vortex gyration as a function of the strength of the external bias field and its angle θ with respect to the x axis determined from micromagnetic simulations of a single triangle. The corresponding magnetic ground state of the triangle with round corners is shown in (b). For comparison, the ground state of a triangle with sharp corners is shown in (c). Arrows indicate the magnetization directions. Both triangles have the chirality $C = -1$.

micromagnetic simulations of the free vortex relaxation at constant bias fields. Note that the results shown in Fig. 4(a) are obtained using a triangle with round corners which reflects the experimental conditions, see Fig. 4(b). For sharp corners, micromagnetic simulations of the ground state reveal an end domain, see Fig. 4(c), which strongly influences the dynamic behavior of the vortex structure (not shown). The magnetization pattern of the lower triangle in Fig. 1(b) observed via x-ray microscopy might reveal characteristics of Fig. 4(c). However, the main part of the x-ray measurements and the very good agreement of the simulations with the FMR data strongly indicate that the pure vortex state is dominantly present in our structures.

In summary, we have shown by non-invasive x-ray microscopy that the chirality of triangular-shaped permalloy structures can be controlled via the direction of an in-plane magnetic field. After nucleation of the vortex state, the magnetization along the edge parallel to the field axis opposes the direction of the field that was applied to initially saturate the sample. The asymmetric magnetic confining potential has been determined via broadband FMR measurements and micromagnetic simulations. It has been shown that the potential reflects the shape of the sample and that it is steeper at the corners in comparison to the edges. Overall, the resonance frequency of vortex gyration has been tuned by about 17% via the application of an external bias field. Their static and dynamic properties make the magnetic triangular-shaped structures a promising candidate for applications and bring along a variety of interesting experiments, e.g., making use of the specific asymmetric confining potential or the magnetostatic coupling together with the tunability of the resonance frequency over a wide range.

We thank Ulrich Merkt for fruitful discussions and continuous support and Michael Volkmann for superb technical assistance. Financial support of the Deutsche Forschungsgemeinschaft via the Sonderforschungsbereich 668 and the Graduiertenkolleg 1286 is gratefully acknowledged. Operation of the x-ray microscope is supported by the Director, Office of Science, Office of Basic Energy Sciences, of the U.S. Department of Energy under Contract No. DE-AC02-05-CH11231.

[1]T. Shinjo *et al.*, Science **289**, 930 (2000).
[2]R. P. Cowburn *et al.*, Phys. Rev. Lett. **83**, 1042 (1999).
[3]R. Antos, Y. Otani, and J. Shibata, J. Phys. Soc. Jpn. **77**, 031004 (2008).
[4]S.-K. Kim *et al.*, Appl. Phys. Lett. **92**, 022509 (2008).
[5]S. Bohlens *et al.*, Appl. Phys. Lett. **93**, 142508 (2008).
[6]A. Vogel *et al.*, Phys. Rev. Lett. **105**, 037201 (2010).
[7]M. Weigand *et al.*, Phys. Rev. Lett. **102**, 077201 (2009).
[8]K. Yamada *et al.*, Appl. Phys. Lett. **93**, 152502 (2008).
[9]M. Kammerer *et al.*, Nature Commun. **2**, 279 (2011).
[10]S. Yakata *et al.*, Appl. Phys. Lett. **97**, 222503 (2010).
[11]M. Jaafar *et al.*, Nanotechnology **19**, 285717 (2008).
[12]M. Jaafar *et al.*, Phys. Rev. B **81**, 054439 (2010).
[13]K. S. Buchanan *et al.*, Nat. Phys. **1**, 172 (2005).
[14]M. Bolte *et al.*, Phys. Rev. Lett. **100**, 176601 (2008).
[15]A. Vogel *et al.*, Phys. Rev. Lett. **106**, 137201 (2011).
[16]S. Sugimoto *et al.*, Phys. Rev. Lett. **106**, 197203 (2011).
[17]A. Vogel *et al.*, Appl. Phys. Lett. **99**, 042506 (2011).
[18]H. Jung *et al.*, Sci. Rep. **1**, 59 (2011).
[19]S. Barman, A. Barman, and Y. Otani, J. Phys. D: Appl. Phys. **43**, 335001 (2010).
[20]J. Shibata and Y. Otani, Phys. Rev. B **70**, 012404 (2004).
[21]M. Miyata *et al.*, J. Appl. Phys. **111**, 07B902 (2012).
[22]P. Monceau and J.-C. S. Lévy, Phys. Lett. A **374**, 1872 (2010).
[23]M. Miyata *et al.*, IEEE Trans. Magn. **47**, 2505 (2011).
[24]P. Fischer *et al.*, Mater. Today **9**, 26 (2006).
[25]C. T. Chen *et al.*, Phys. Rev. B **42**, 7262 (1990).
[26]J. Podbielski, F. Giesen, and D. Grundler, Phys. Rev. Lett. **96**, 167207 (2006).
[27]A. A. Thiele, Phys. Rev. Lett. **30**, 230 (1973).
[28]B. Krüger *et al.*, Phys. Rev. B **76**, 224426 (2007).
[29]A. Drews *et al.*, Phys. Rev. B **85**, 144417 (2012).
[30]K. Y. Guslienko, R. Hernández Heredero, and O. Chubykalo-Fesenko, Phys. Rev. B **82**, 014402 (2010).
[31]H. H. Langner *et al.*, Phys. Rev. B **85**, 174436 (2012).
[32]K. S. Buchanan *et al.*, Phys. Rev. B **74**, 064404 (2006).
[33]See http://micromagnum.informatik.uni-hamburg.de.

DISCLAIMER

This document was prepared as an account of work sponsored by the United States Government. While this document is believed to contain correct information, neither the United States Government nor any agency thereof, nor The Regents of the University of California, nor any of their employees, makes any warranty, express or implied, or assumes any legal responsibility for the accuracy, completeness, or usefulness of any information, apparatus, product, or process disclosed, or represents that its use would not infringe privately owned rights. Reference herein to any specific commercial product, process, or service by its trade name, trademark, manufacturer, or otherwise, does not necessarily constitute or imply its endorsement, recommendation, or favoring by the United States Government or any agency thereof, or The Regents of the University of California. The views and opinions of authors expressed herein do not necessarily state or reflect those of the United States Government or any agency thereof or The Regents of the University of California.

This work was supported by the Director, Office of Science, of the U.S. Department of Energy under Contract No. DE-AC02-05CH11231.